IEEE Access
Multidisciplinary | Rapid Review | Open Access Journal

Received 1 February 2024, accepted 8 March 2024, date of publication 18 March 2024, date of current version 28 March 2024.

Digital Object Identifier 10.1109/ACCESS.2024.3379137

RESEARCH ARTICLE

Energy-Efficient Forward-Biased PIN Silicon Mach–Zehnder Modulator With 50 μm Active Phase Shifter Length

SOURAV DEV[1], KARANVEER SINGH[2], MIRCEA CATUNEANU[1], HRISHIKESH VITHALANI[1], ABHINAND VENUGOPALAN[2], JANOSCH MEIER[2], THOMAS SCHNEIDER[2], AND KAMBIZ JAMSHIDI[1], (Senior Member, IEEE)

[1]Integrated Photonic Devices Group, Technische Universität Dresden, 01609 Dresden, Germany
[2]THz-Photonics Group, Technische Universität Braunschweig, 38106 Braunschweig, Germany

Corresponding author: Sourav Dev (sourav.dev@tu-dresden.de)

This work was supported in part by German Research Foundation (Deutsche Forschungsgemeinschaft, DFG) under Grant 403579441, Grant 424608109, Grant 424608271, Grant 424607946, Grant 424608191, Grant 403154102, Grant 322402243, Grant 454954953, and Grant 491066027; in part by German Federal Ministry of Education and Research (Bundesministerium für Bildung und Forschung, BMBF) under Grant 16KISQ119 and Grant 16KISK001K; and in part by the Open Access Publication Funds of Technische Universität Dresden.

ABSTRACT We present the design performance validation of an energy-efficient silicon Mach-Zehnder modulator (MZM) with a forward-biased PIN junction by simulation and experiment. With a length of 50 μm, the presented MZM exhibits at least four times smaller form factor for the active phase-shifter than the state-of-the-art. Furthermore, we recorded a remarkably low $V_\pi L$ of only 0.0025 V$\times$cm. By thermal tuning of an additional heater, segmented with the phase shifter, the measured DC extinction ratio of the MZM was 30 dB. Non-return-to-zero data transmission up to 5 Gb/s and the generation of sinc-shaped Nyquist pulse sequences with a bandwidth of 12 GHz is demonstrated. The very small footprint and power consumption make the presented MZM an ideal choice for various applications like Nyquist pulse generation, parallel analog signal processing, arbitrary waveform generation, etc.

INDEX TERMS Electro-optic modulators, photonic integrated circuits, silicon photonics.

I. INTRODUCTION

In recent years, the demand for large-scale integration has been increasing [1], [2]. Due to their compatibility with the existing complementary metal-oxide-semiconductor (CMOS) technology, integrated silicon-on-insulator (SOI) electro-optic modulators have already been subjected to a lot of research [3]. One such device is a Mach-Zehnder modulator (MZM) which is based on a Mach-Zehnder interferometer. In one or both interferometer arms the optical path is changed by a modulation-signal dependent phase change. This phase change is transferred to an intensity change of the optical wave by the interference between both arms. The modulation efficiency of the MZM can be calculated by the performance metric $V_\pi L$, with V_π as the required voltage to achieve a phase shift of π. In silicon MZM there are several ways to obtain a phase shift like the plasma dispersion effect, where an external voltage is applied to change the free-carrier concentration [4], [5]. This voltage can be applied in the forward or reverse-biased direction. Depending on the system requirements, different configurations of MZMs can be designed. Up to now, in the field of optical communications, the preference has been predominantly towards the reversed-biased configuration, since these modulators can provide high bandwidths and therefore, high-speed communications [6], [7], [8], [9]. However, in addition to their applications in optical communications, MZMs have attracted a lot of attention to be utilized in various other fields like microwave photonics [10], LiDAR [11], [12], quantum key distribution [13], [14], optical switches [15], [16], optical computing like reservoir computing [17], [18], etc. Some of these fields, for example, LiDAR do not require

The associate editor coordinating the review of this manuscript and approving it for publication was Stanley Cheung.

high bandwidth or modulation speed in the GHz range and should be operated with low power consumption [11], [12]. However, they need large-scale integration. To satisfy these requirements, forward-biased MZMs become advantageous because they offer low power consumption as well as low insertion loss (IL) [19], [20], [21], [22], [23], [24], [25]. Forward-biased modulators are also comparatively smaller in size and thus can be helpful for large-scale integration.

The performance of a modulator can be improved in terms of different figures of merit using special structures. For example, silicon-based ring modulators provide a low form factor. However, they lack thermal stability in a densely packed network of photonic integrated circuits [26]. Alternatively, an MZM can be modified into compact structures like corrugated modulators, but the trade-off here is high insertion loss [27], [28], [29], [30], [31]. However, to reduce the design and operation complexity, standard MZMs can be a very good choice. Standard MZMs while integrated can be directly utilized as analog to digital converters (ADC), arbitrary waveform generators (AWG), Nyquist pulse generators, etc. [32], [33], [34].

TABLE 1. Comparison of the performance metrics for forward-biased standard MZM.

Ref.	Phase shifter length (μm)	$V_\pi L$ [a] (V×cm)	ER (dB) in DC	Power Consumption (mW/Gb/s)	IL (dB)	Speed (Gb/s)
[22]	200	0.036	10	5.1	12	10
[23]	250	0.024	16	N.A.	N.A.	10
[24]	250	0.29	23	N.A.	1.2	12.5
[25] [b]	250	0.1	N.A.	0.6	7.2	50
[31] [b]	250	0.075	N.A.	1.2	4.6	56
[20]	500	0.07	33	0.88	2.5 [c]	15
This work	50	0.0025	30	4.12	1.2	5

[a] V_π is the voltage required for a π phase shift.
[b] Including driver/equalizer
[c] Calculated value (excluding grating coupler and MMI loss)

In this paper, we present the characterization and design of a silicon MZM with a forward-biased PIN junction. The active phase-shifter length of this modulator is 50 μm. To the best of our knowledge, this is the shortest reported active phase shifter length for an MZM so far. An overview of forward-biased ultra-compact modulators with high ER along with low $V_\pi L$ is presented in Table 1. The presented modulator can achieve a high extinction ratio (ER) of 30 dB, which is very close to the DC ER of our previously reported forward-biased modulator (33 dB but with a 10 times longer active phase shifter length [20]) and 7 dB higher compared to other reported modulators. We also demonstrate that our modulator can transmit data with a bitrate of 5 Gb/s. This is lower than our previously reported 15 Gb/s modulator [20]. However, due to the very short active phase-shifter length, more devices can be accommodated in the same area. This is especially important for integrated parallel systems, which utilize parallelization of the silicon modulators for high bandwidth signal generation or reception with low-speed electronics and photonics on a fully integrated module [35], [36]. Since these methods are based on Nyquist sinc-pulse sequences, we also demonstrate our modulator as an integrated Nyquist pulse generator.

The paper is structured as follows. In section II, the design of the modulator is discussed together with static and direct current (DC) characterizations. The evaluation of the radio frequency (RF) characterization is presented in section III. In section IV, the results for Nyquist pulse generation are demonstrated and, finally, the paper is concluded in section V.

II. DESIGN AND DC CHARACTERIZATION

The cross-section of the modulator is designed based on a simulation to maximize the change of refractive index and subsequently the phase shift with a certain applied voltage, as well as to keep the linear loss to a tolerable level.

For evaluation, several cross-sections like PN and PIN with various intrinsic region widths were simulated. The length of the active phase shifter was fixed to 50 μm to minimize the size of the MZM. As the chips were fabricated by the Advanced Micro Foundry (AMF), the thickness and width of the rib waveguide are 220 nm and 500 nm respectively, as per the foundry standard. The doping concentration, buried oxide thickness, etc. were also selected according to the foundry specifications. The simulations were carried out with the Lumerical software package, considering forward-biased configuration. The voltage is swept from 0 to 3.4 V.

First, the charge distribution for these cross-sections was evaluated by a static simulation with the DEVICE package. The surface recombination is set to 10^7cm/s and is considered a boundary condition. The same cross-section is also simulated by the MODE package. The mode profile is computed by importing the charge distribution achieved in the previous step. To optimize the modulator design, simulations considering several cross-sections were carried out. We simulated five different designs with various widths of the intrinsic region. We started with zero (PN-junction diode), and then we gradually increased the width to 2.5 μm. The results are presented in Fig. 1. As can be seen in Fig. 1(a), the highest phase shifts can be achieved for high bias voltages and low widths of the intrinsic region. However, this results in a higher loss (as depicted in Fig. 1(b)). Other very important parameters, i.e. junction capacitance and resistance were simulated for the same voltage range and are presented in Fig. 1(c) for the five cross-section designs mentioned before. It is evident from Fig. 1(c) that the junction capacitances increase as the PIN diode turns on. After it reaches a maximum at a certain voltage, the capacitance decreases slowly and will gradually reach a saturation point at higher bias voltages. Fig. 1(c) also shows the behavior of the junction resistances. While the value of the resistance is very high when the PIN diode is off, it starts to decrease exponentially as the PIN diode turns on around 0.7 V. Additionally, the resistance of the junction decreases with

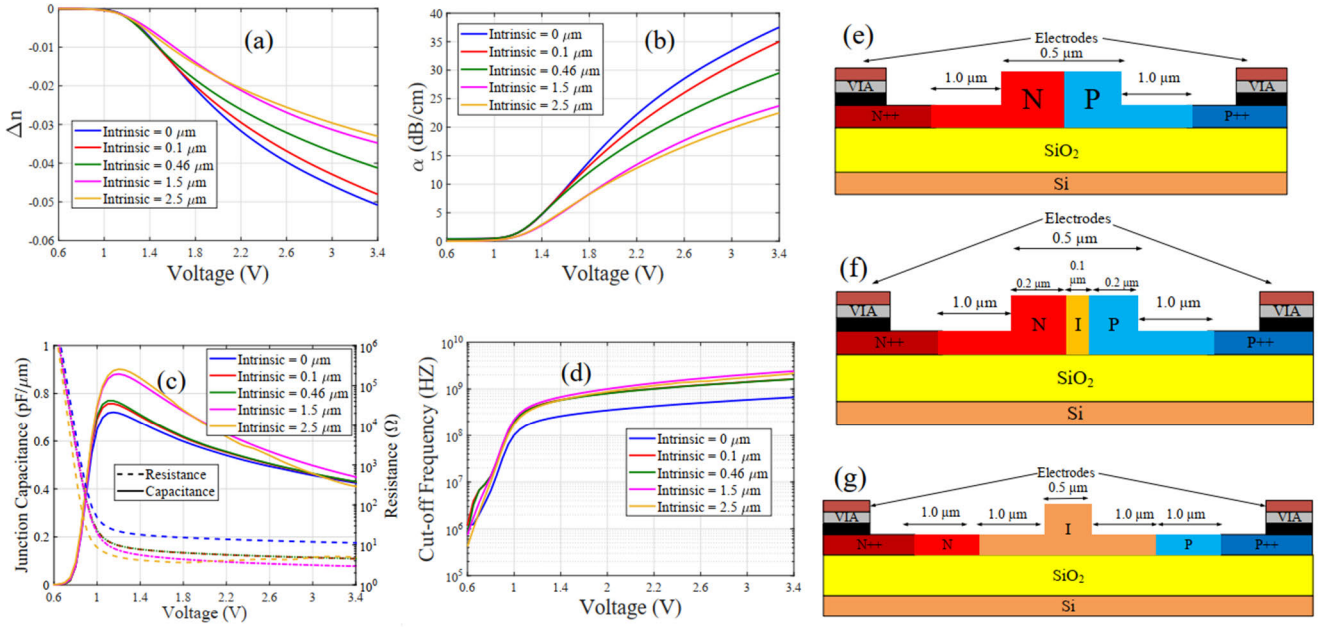

FIGURE 1. Cross-section analysis. Subfigures (a)-(d) present different parameters against the applied bias voltage for 5 different cross sections which varies the width of the intrinsic region. (a) Change of refractive index vs. voltage, (b) linear loss vs. voltage, (c) Resistance and capacitance vs. voltage, and (d) Cut-off frequencies vs. voltage. Intrinsic = 0 μm corresponds to a PN-junction diode, which is shown in (e). Intrinsic = 0.1 and 0.46 μm mean that there is an intrinsic region of various lengths in the middle of the waveguide, as shown in (f) for 0.1 μm. For an intrinsic width of 2.5 μm, the whole WG and 1 μm on each side of the WG (in the slab regions) belong to the intrinsic region, which is shown in (g).

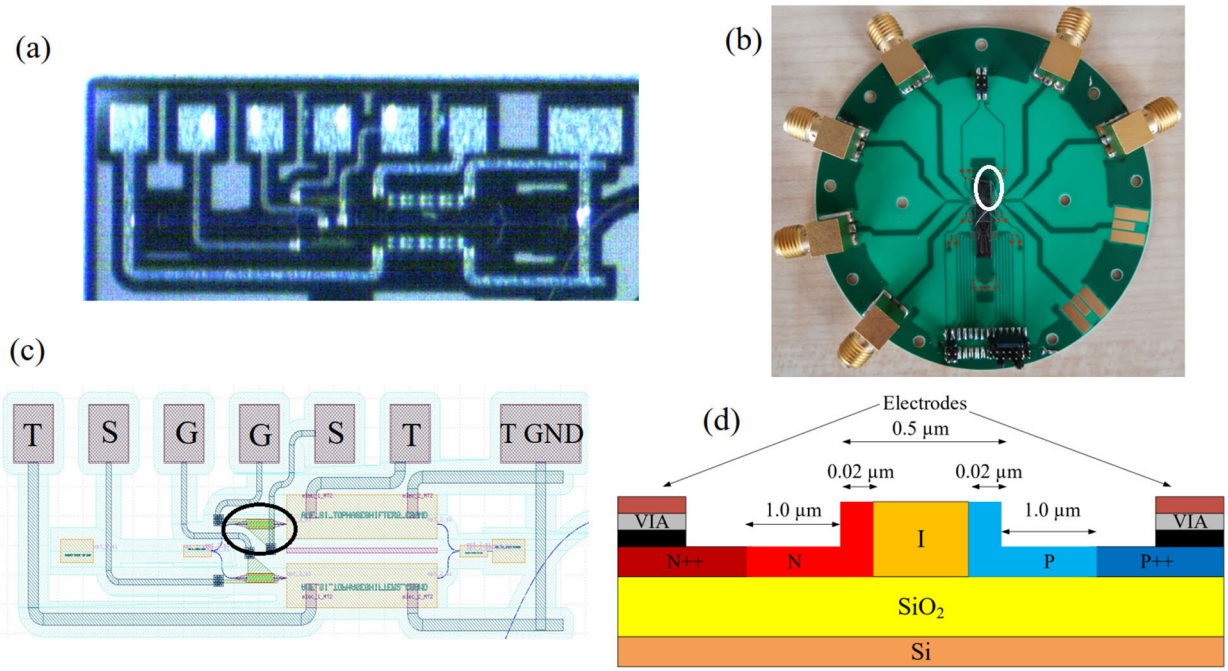

FIGURE 2. (a) Microscope image of the fabricated MZM, (b) PCB with the fabricated chip glued on it (the white circle indicates where the modulator is placed), (c) Detailed top view of the circuit (GDS layout) including the modulator. The black circle marks the active phase shifter in one arm of the modulator, (d) A cross-sectional view of the active phase shifter for the fabricated MZM.

the increase of the intrinsic widths. However, the junction capacitance keeps increasing with the increase of the intrinsic width. Fig. 1(d) presents the cut-off frequencies against the bias voltage based on the junction capacitance and resistance values. It shows the limitation of the cut-off frequency of the forward-biased modulator which is limited to around 1 GHz.

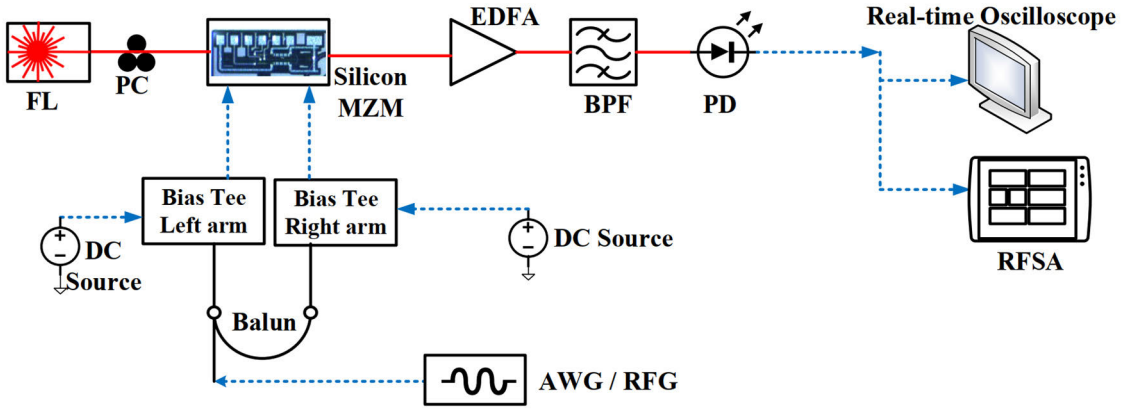

FIGURE 3. Experimental setup for the characterization of the integrated modulator wire-bonded on a PCB; FL: fiber laser, PC: polarization controller, AWG/RFG: arbitrary waveform generator or radio-frequency generator, respectively, two DC sources are used for two arms of the modulator, subsequently two bias tees are used to combine DC and RF input for two arms of the modulator, the Balun splits the AWG/RFG into two parts to be fed into two bias tees. EDFA: Erbium-doped fiber amplifier, BPF: bandpass filter, PD: photodiode, RFSA: radio-frequency spectrum analyzer. The red lines are optical paths, and the dotted blue ones are electrical paths.

Comparing all five configurations, a trade-off was made and the PIN cross-section with a 0.46 μm of intrinsic width was chosen for fabrication. The final cross-section of the active phase shifter is presented in Fig. 2(d).

In the next step, the fabricated chips were characterized. Several chips were used for the initial DC characterization to ensure the correctness of the results. All the chips provided almost similar results. Therefore, we randomly chose one of them for wire bonding on a printed circuit board (PCB) for further investigation. The fabricated chip wire-bonded and glued on a printed circuit board (PCB) is shown in Fig. 2(b). Only the results acquired from this single chip, achieved with the setup in Fig. 3, are reported here. As an optical source, a fiber laser (FL) from NKT Photonics with a center wavelength of 1550.116 nm and an optical power of 12.3 dBm was used. A grating coupler (GC) on the chip couples the light into the modulator. A polarization controller (PC) ensures the polarization alignment. The coupling losses of the input and output couplers were measured with a reference waveguide placed on the same chip to be 15.4 dB. The output power was measured to be −4.3 dBm, which corresponds to a total optical loss of the forward-biased silicon modulator of 1.2 dB.

Two bias tees were used at the two arms of the modulator to combine the DC and the input electrical signals and pass them to the electrical ports of the modulator. As depicted in Fig. 2(c), each phase shifter of the modulator has one ground (G) and one signal (S) port. These two ports work as RF and DC input ports. One additional DC port (T) at each arm of the modulator is utilized for thermal tuning. For both thermal tuning ports, there is a common ground (T GND). One arm of the modulator receives a fixed voltage, where the voltage is swept using the signal port on the other arm. RF and DC connectors are soldered on the PCB for this purpose. To compensate for the coupling losses, an Erbium-doped fiber amplifier (EDFA) followed by a bandpass filter (BPF) for filtering out the amplified spontaneous emission noise was used at the output. The signal was detected with a 40 GHz Photodiode from Optilab.

In Fig. 4, the DC characterization results without any thermal tuning are presented in comparison with the simulation for the current-voltage (IV)-characteristics and the output optical power of the modulator. Here, the normalized transmission through the MZM was simulated considering the plasma dispersion effect. The normalized transmission is evaluated using Eq. (1).

In Eq. (1) σ is the splitting ratio (the ratio of the power in each phase-shifter), L_1 and L_2 are the lengths of the two arms, and n_{eff1}, and n_{eff2} are their refractive indices, respectively. V_1 and V_2 represent the voltage applied to the respective arms. The detailed analysis of this equation is discussed in our previous publication [20].

$$T_0(V_1, V_2) = \left|\frac{1}{1+\sigma}\left(\sigma \exp\left(-\frac{2\pi}{\lambda_o} n_{eff\,1}(V_1) L_1\right) + \exp\left(-\frac{2\pi}{\lambda_o} n_{eff\,2}(V_2) L_2\right)\right)\right|^2 \quad (1)$$

Figure 4(b) represents the change of the output optical power as a function of the applied bias voltage for an optical input power of 12 dBm. As shown, the simulation and experimental results fairly match. By changing the bias of the active phase shifters, we get the first transmission minimum with an ER of 10 dB around 2.5 V for a current of 15 mA (Fig. 4(a)). The second transmission minimum appears around 3 V. That means the difference between the two dips is 0.5 V, which corresponds to the required voltage for the π-phase shift. Therefore, the $V_\pi L$ of this modulator can be assumed as 0.5 V × 50 μm = 0.0025 V×cm, which to the best of our knowledge is the lowest $V_\pi L$ reported for forward-biased Mach-Zehnder modulators.

In the next step, thermal tuning is applied to improve the ER. The result is presented in Fig. 5. In this case the voltage

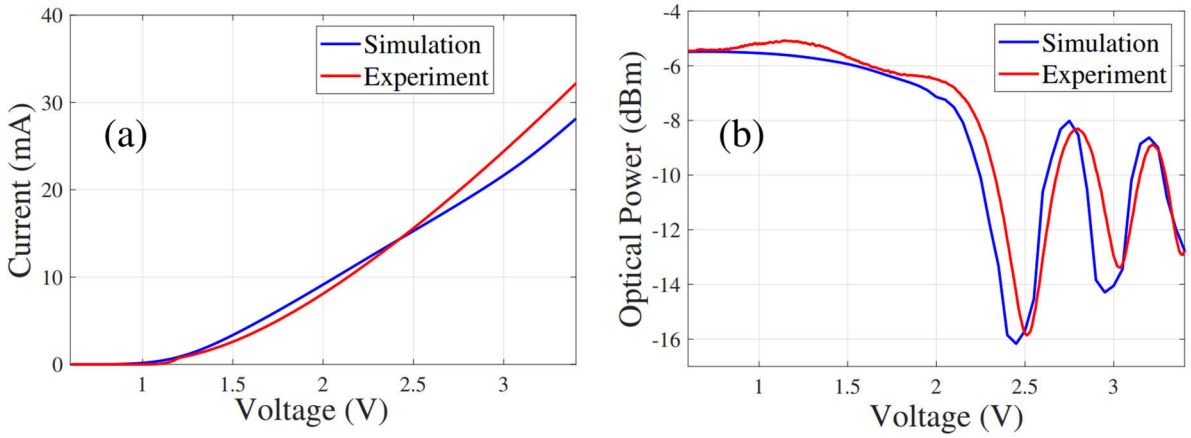

FIGURE 4. DC characterization of the MZM for different bias voltages: (a) current-voltage characteristics, (b) transmitted optical power as a function of the applied voltage without any thermal tuning.

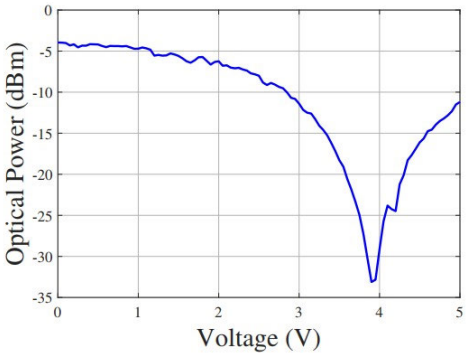

FIGURE 5. Transmitted optical power of the modulator as a function of the applied bias voltage with active thermal tuning.

required at the phase-shifter for the π phase-shift is 3.8 V. However, the DC ER in this case is about 30 dB and the transfer function is more linear. The change in the ER is due to an imbalance (length or width) between the two arms, which results in different phase shifts induced by each arm [20]. When there are some imbalances, the arm of the modulator used for modulating may already have a phase shift induced. This means the transmission maxima might start with a lower value than expected, which subsequently results in a lower ER. With thermal tuning, this imbalance can be compensated, and the transmission maximum starts with the expected value (balanced arms), resulting in a higher ER.

III. RF CHARACTERIZATIONS OF THE MZM

With an RF signal generator (Agilent Technologies E8257D) as electrical input to the MZM, we measured the BW and the data modulation speed of the modulator. The electrical input power of the modulator for the frequency sweep from 100 kHz to 5 GHz was 5 dBm or 1.125 Vpp. A radio frequency spectrum analyzer measures the electro-optic response of the modulator. The measurement result in comparison to the simulation with Lumerical INTERCONNECT is presented in Fig. 6(a). Due to the forward-biased operation, the roll-off is fast. Therefore, the 3-dB BW is around 500 MHz, and the 10-dB BW is 1 GHz.

In the next step, the data modulation capability of the modulator was evaluated. An arbitrary waveform generator (AWG) generates a non-return-to-zero (NRZ) PRBS-7 binary phase shift keying modulation (BPSK) signal. Here an electrical amplifier with 26 dB gain was used to amplify the electrical signal generated by the AWG to a modulator input power of 8 dBm. The bias was set to 2V, to remain in the linear zone of the π-phase shift curve of the modulator shown in Fig. 4. This method reduces the DC power consumption, although it needs a higher RF swing voltage. Different peak-to-peak voltage swings were applied to find the lowest possible bit error rate (BER). Here the lowest BER was found for the swing of 1.125 V_{pp}. The electrical signal was converted to an optical signal and measured by a 20 GHz photodiode. To track and analyze the waveform in real-time, a real-time oscilloscope (Tektronix DPO73304) was utilized. All analyses were conducted for 3 Gb/s, 4 Gb/s, and 5 Gb/s NRZ PRBS-7 BPSK modulations.

TABLE 2. Comparison of the performance metrics.

NRZ bit rate (Gb/s)	Q-factor	BER	EVM
3	11.5	8.51e-05 [a]	26 %
4	11.2	3.29e-04	26.6 %
5	10.3	4.34e-04	30.18 %

[a] calculated BER

The recorded eye diagrams are presented in Fig. 6 (b), (c), and (d). In the case of 3 Gb/s, no bit error was recorded for the transmission of 15,000 bits. Therefore, the BER is calculated from the measured Q-factor [37]. To compare the performance metrics, the Q-factors, BERs, and EVM are presented in Table 2. Considering 5 Gb/s speed, the power consumption is calculated to be 4.12 mW/Gb/s. All the performances reported in this manuscript can be improved

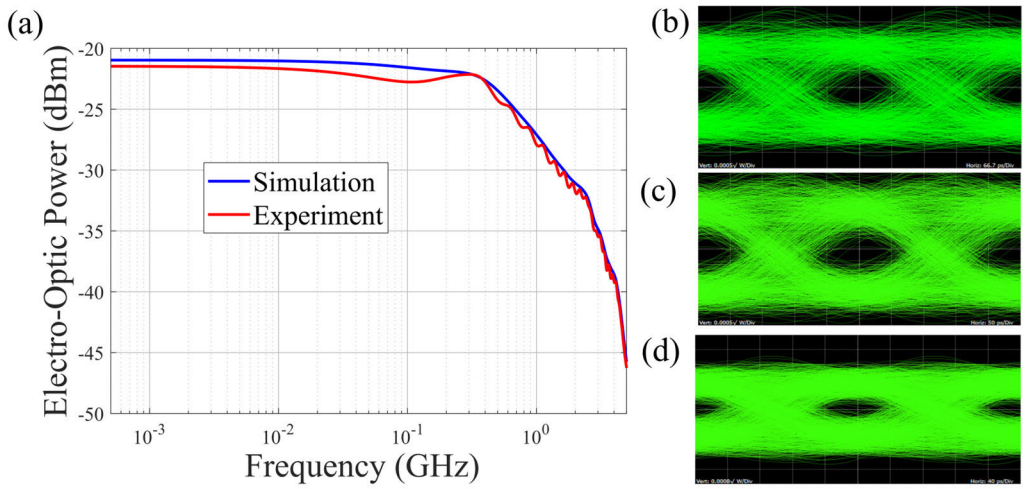

FIGURE 6. (a) Measured and simulated electro-optic output power. Measured eye diagrams for a non-return-to-zero (NRZ) PRBS-7 data modulation for (b) 3 Gb/s, (c) 4 Gb/s, and (d) 5 Gb/s.

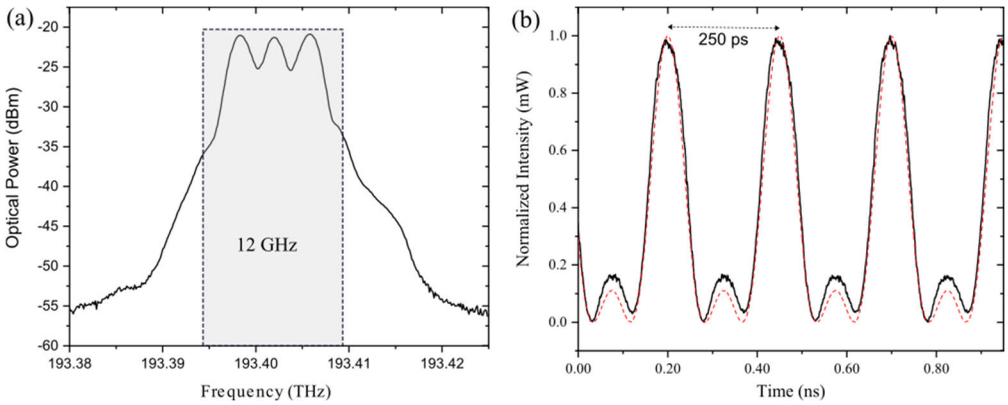

FIGURE 7. (a) 4 GHz input signal, (b) Generation of 12 GHz Nyquist pulses. The solid black line represents the experimentally generated pulses, while the dashed red line represents the mathematically calculated ideal sinc pulse.

by pre-distorting the signal with an arbitrary waveform generator. However, we did not use any electronic pre- or post-processing to show the real performance of this modulator.

IV. MZM AS NYQUIST PULSE GENERATOR

A sinc pulse sequence is the unlimited summation of ideal sinc pulses with a distinct time shift [34] and is just a rectangular frequency comb, which can be generated quite easily by driving the modulator with n equally spaced electrical input frequencies [35], [38]. Such sinc-pulse sequences can be used to down-convert high-bandwidth signals into several parallel low-bandwidth ones, which can then be processed with low-bandwidth electronics [34]. Due to its compactness, the presented modulator can be very beneficial for such an application. Therefore, we show how it can be used for the generation of sinc-pulse sequences.

Figure 7(b) shows a sinc pulse sequence with two zero crossings (one sinusoidal input frequency and a DC bias) generated by the modulator (black solid) compared to the calculated ideal trace (red dashed). As can be seen, although the 3dB bandwidth of the modulator is just 0.5 GHz, it can be used to generate sinc pulse sequences with a bandwidth of up to 12 GHz, which corresponds to a pulse width of 250 ps. Therefore, the modulator can be used for the processing of signals with a symbol rate of 12 GBd [39].

We previously demonstrated Nyquist pulse generation using reverse-biased on-chip modulators with lengths of 3.2 and 1 mm [32], [33]. The demonstration in this paper proves that an ultra-compact forward-biased MZM with an active phase shifter length in the micrometer range can also be utilized for Nyquist pulse generation. Therefore, it is possible to take advantage of the compact size of the active phase shifter to accommodate more modulators in the same chip area, which is especially important for parallel signal processing based on Nyquist pulses. The presented silicon modulator enables high-bandwidth pulse generation with the smallest possible silicon footprint presented till now.

Therefore, it is an ideal candidate for designing photonic DAC and ADC [36].

V. CONCLUSION

We have demonstrated, for the first time, to the best of our knowledge, a forward-biased PIN junction-based silicon MZM with an active phase shifter length of only 50 μm which is able to modulate normal data at 5 Gb/s. This modulator can be utilized to process signals with symbol rates up to 12 GBd by orthogonal sampling. With thermal tuning, the modulator can achieve a high DC ER of 30 dB. The MZM also has a very low insertion loss of 1.2 dB and a good modulation efficiency ($V_\pi L$) of 0.0025 V.cm.

REFERENCES

[1] S. Y. Siew, B. Li, F. Gao, H. Y. Zheng, W. Zhang, P. Guo, S. W. Xie, A. Song, B. Dong, L. W. Luo, C. Li, X. Luo, and G.-Q. Lo, "Review of silicon photonics technology and platform development," *J. Lightw. Technol.*, vol. 39, no. 13, pp. 4374–4389, Jul. 13, 2021.

[2] G. T. Reed and C. E. Jason Png, "Silicon optical modulators," *Mater. Today*, vol. 8, no. 1, pp. 40–50, Jan. 2005.

[3] J. Witzens, "High-speed silicon photonics modulators," *Proc. IEEE*, vol. 106, no. 12, pp. 2158–2182, Dec. 2018.

[4] M. Nedeljkovic, R. Soref, and G. Z. Mashanovich, "Free-carrier electrorefraction and electroabsorption modulation predictions for silicon over the 1–14-μm infrared wavelength range," *IEEE Photon. J.*, vol. 3, no. 6, pp. 1171–1180, Dec. 2011.

[5] S. Sabouri, L. A. M. Velasco, M. Catuneanu, M. Namdari, and K. Jamshidi, "Thermo optical phase shifter with low thermal crosstalk for SOI strip waveguide," *IEEE Photon. J.*, vol. 13, no. 2, pp. 1–12, Apr. 2021.

[6] S. J. Spector, M. W. Geis, G.-R. Zhou, M. E. Grein, F. Gan, M. A. Popović, J. U. Yoon, D. M. Lennon, E. P. Ippen, F. X. Kärtner, and T. M. Lyszczarz, "CMOS-compatible dual-output silicon modulator for analog signal processing," *Opt. Exp.*, vol. 16, no. 15, p. 11027, 2008.

[7] M. Passoni, D. Gerace, L. O'Faolain, and L. C. Andreani, "Slow light with interleaved p-n junction to enhance performance of integrated Mach–Zehnder silicon modulators," *Nanophotonics*, vol. 8, no. 9, pp. 1485–1494, Sep. 2019.

[8] O. Jafari, W. Shi, and S. Larochelle, "Mach–Zehnder silicon photonic modulator assisted by phase-shifted Bragg gratings," *IEEE Photon. Technol. Lett.*, vol. 32, no. 8, pp. 445–448, Apr. 5, 2020.

[9] C. Kress, K. Singh, T. Schwabe, S. Preußler, T. Schneider, and J. C. Scheytt, "High modulation efficiency segmented Mach–Zehnder modulator monolithically integrated with linear driver in 0.25 μm BiCMOS technology," in *Proc. OSA Adv. Photon. Congr.*, 2021, pp. 1–12.

[10] D. Marpaung, C. Roeloffzen, R. Heideman, A. Leinse, S. Sales, and J. Capmany, "Integrated microwave photonics," *Laser Photon. Rev.*, vol. 7, no. 4, pp. 506–538, Jul. 2013.

[11] W. Yi, Z. Li, Z. Zhou, E. Sillekens, T. Gerard, C. Deakin, F. M. Ferreira, L. Galdino, Z. Liu, P. Bayvel, and R. I. Killey, "Frequency-modulated chirp signals for single-photodiode based coherent LiDAR system," *J. Lightw. Technol.*, vol. 39, no. 14, pp. 4661–4670, Jul. 15, 2021.

[12] Z. Xu, L. Tang, H. Zhang, and S. Pan, "Simultaneous real-time ranging and velocimetry via a dual-sideband chirped LiDAR," *IEEE Photon. Technol. Lett.*, vol. 29, no. 24, pp. 2254–2257, Dec. 15, 2017.

[13] A. A. E. Hajomer, N. Jain, H. Mani, H.-M. Chin, U. L. Andersen, and T. Gehring, "Modulation leakage-free continuous-variable quantum key distribution," *npj Quantum Inf.*, vol. 8, no. 1, pp. 1–8, Nov. 2022.

[14] J. L. O'brien, A. Furusawa, and J. Vuč ković, "Photonic quantum technologies," *Nature Photon. 3*, vol. 3, no. 12, pp. 687–695, 2009.

[15] N. Dupuis, B. G. Lee, A. V. Rylyakov, D. M. Kuchta, C. W. Baks, J. S. Orcutt, D. M. Gill, W. M. J. Green, and C. L. Schow, "Design and fabrication of low-insertion-loss and low-crosstalk broadband 2 × 2 Mach–Zehnder silicon photonic switches," *J. Lightw. Technol.*, vol. 33, no. 17, pp. 3597–3606, Sep. 7, 2015.

[16] M. R. Watts, J. Sun, C. DeRose, D. C. Trotter, R. W. Young, and G. N. Nielson, "Adiabatic thermo-optic Mach–Zehnder switch," *Opt. Lett.*, vol. 38, no. 5, pp. 733–735, 2013.

[17] M. Nakajima, K. Tanaka, and T. Hashimoto, "Scalable reservoir computing on coherent linear photonic processor," *Commun. Phys.*, vol. 4, no. 1, pp. 1–12, Feb. 2021.

[18] J. Qin, Q. Zhao, H. Yin, Y. Jin, and C. Liu, "Numerical simulation and experiment on optical packet header recognition utilizing reservoir computing based on optoelectronic feedback," *IEEE Photon. J.*, vol. 9, no. 1, pp. 1–11, Feb. 2017.

[19] R. L. Chao, J. W. Shi, A. Jain, T. Hirokawa, A. S. P. Khope, C. Schow, J. E. Bowers, R. Helkey, and J. F. Buckwalter, "Forward bias operation of silicon photonic Mach zehnder modulators for RF applications," *Opt. Exp.*, vol. 25, no. 19, p. 23181, 2017.

[20] S. Dev, K. Singh, R. Hosseini, A. Misra, M. Catuneanu, S. Preußler, T. Schneider, and K. Jamshidi, "Compact and energy-efficient forward-biased PN silicon Mach–Zehnder modulator," *IEEE Photon. J.*, vol. 14, no. 2, pp. 1–7, Apr. 2022.

[21] S. Dev, K. Singh, M. Catuneanu, H. Vithalani, A. Venugopalan, M. I. Hosni, T. Schneider, and K. Jamshidi, "Ultra-compact forward-biased PIN silicon Mach–Zehnder modulator with thermal tuning," in *Proc. CLEO*, 2023, pp. 1–2.

[22] W. M. Green, M. J. Rooks, L. Sekaric, and Y. A. Vlasov, "Ultra-compact, low RF power, 10 Gb/s silicon Mach–Zehnder modulator," *Opt. Exp.*, vol. 15, no. 25, p. 17106, 2007.

[23] G.-R. Zhou, M. W. Geis, S. J. Spector, F. Gan, M. E. Grein, R. T. Schulein, J. S. Orcutt, J. U. Yoon, D. M. Lennon, T. M. Lyszczarz, E. P. Ippen, and F. X. Käertner, "Effect of carrier lifetime on forward-biased silicon Mach–Zehnder modulators," *Opt. Exp.*, vol. 16, no. 8, p. 5218, 2008.

[24] S. Akiyama, T. Baba, M. Imai, T. Akagawa, M. Takahashi, N. Hirayama, H. Takahashi, Y. Noguchi, H. Okayama, T. Horikawa, and T. Usuki, "12.5-gb/s operation with 029-Vcm V_πL using silicon Mach–Zehnder modulator based-on forward-biased pin diode," *Optical Express*, vol. 20, no. 3, pp. 2911–2923, 2012.

[25] S. Akiyama, M. Imai, T. Baba, T. Akagawa, N. Hirayama, Y. Noguchi, M. Seki, K. Koshino, M. Toyama, T. Horikawa, and T. Usuki, "Compact PIN-diode-based silicon modulator using side-wall-grating waveguide," *IEEE J. Sel. Topics Quantum Electron.*, vol. 19, no. 6, pp. 74–84, Nov. 2013.

[26] M. I. Hosni, K. Singh, Y. Mandalawi, T. Schneider, and A. M. Mokhtar, "Compact agnostic Nyquist WDM transmission system based on cascaded silicon ring modulators," in *Proc. Asia Commun. Photon. Conf. (ACP)*, Shenzhen, China, Nov. 2022, pp. 526–529.

[27] Y. Hinakura, H. Arai, and T. Baba, "64 gbps Si photonic crystal slow light modulator by electro-optic phase matching," *Opt. Exp.*, vol. 27, no. 10, p. 14321, 2019.

[28] A. Brimont, D. J. Thomson, P. Sanchis, J. Herrera, F. Y. Gardes, J. M. Fedeli, G. T. Reed, and J. Martí, "High speed silicon electro-optical modulators enhanced via slow light propagation," *Opt. Exp.*, vol. 19, no. 21, p. 20876, 2011.

[29] R. Hosseini, A. Khachaturian, M. Cătuneanu, P. P. Khial, R. Fatemi, A. Hajimiri, and K. Jamshidi, "Compact, high extinction ratio silicon Mach–Zehnder modulator with corrugated waveguides," in *Proc. Conf. Lasers Electro-Optics (CLEO)*, San Jose, CA, USA, May 2018, pp. 1–2.

[30] R. Hosseini, L. Mirzoyan, and K. Jamshidi, "Energy consumption enhancement of reverse-biased silicon-based Mach–Zehnder modulators using corrugated slow light waveguides," *IEEE Photon. J.*, vol. 10, no. 1, pp. 1–7, Feb. 2018.

[31] S. Tanaka, T. Usuki, and Y. Tanaka, "Accurate SPICE model of forward-biased silicon PIN Mach–Zehnder modulator for an energy-efficient multilevel transmitter," *J. Lightw. Technol.*, vol. 36, no. 10, pp. 1959–1969, May 5, 2018.

[32] A. Misra, C. Kress, K. Singh, S. Preußler, J. C. Scheytt, and T. Schneider, "Integrated source-free all optical sampling with a sampling rate of up to three times the RF bandwidth of silicon photonic MZM," *Opt. Exp.*, vol. 27, no. 21, p. 29972, 2019.

[33] A. Misra, R. Hosseini, S. Dev, K. Jamshidi, and T. Schneider, "Flexible Nyquist pulse sequence generation from an integrated slow-light silicon modulator for elastic network applications," in *Proc. Photonic Netw., ITG-Symp.*, Nov. 2020, pp. 1–5.

[34] M. A. Soto, M. Alem, M. Amin Shoaie, A. Vedadi, C.-S. Brès, L. Thévenaz, and T. Schneider, "Optical sinc-shaped Nyquist pulses of exceptional quality," *Nature Commun.*, vol. 4, no. 1, pp. 1–11, Dec. 2013.

[35] J. Meier, K. Singh, A. Misra, S. Preußler, J. C. Scheytt, and T. Schneider, "High-bandwidth arbitrary signal detection using low-speed electronics," *IEEE Photon. J.*, vol. 14, no. 2, pp. 1–7, Apr. 2022.

[36] K. Singh, J. Meier, A. Misra, S. Preußler, J. C. Scheytt, and T. Schneider, "Photonic arbitrary waveform generation with three times the sampling rate of the modulator bandwidth," *IEEE Photon. Technol. Lett.*, vol. 32, no. 24, pp. 1544–1547, Dec. 6, 2020.
[37] W. Freude, R. Schmogrow, B. Nebendahl, M. Winter, A. Josten, D. Hillerkuss, S. Koenig, J. Meyer, M. Dreschmann, M. Huebner, C. Koos, J. Becker, and J. Leuthold, "Quality metrics for optical signals: Eye diagram, Q-factor, OSNR, EVM and BER," in *Proc. 14th Int. Conf. Transparent Opt. Netw. (ICTON)*, Jul. 2012, pp. 1–4.
[38] M. A. Soto, M. Alem, M. A. Shoaie, A. Vedadi, C. S. Brès, L. Thèvenaz, and T. Schneider, "Generation of Nyquist sinc pulses using intensity modulators," in *Proc. CLEO*, 2013, pp. 1–2.
[39] A. Misra, J. Meier, S. Preussler, K. Singh, and T. Schneider, "Agnostic sampling transceiver," *Opt. Exp.*, vol. 29, no. 10, p. 14828, 2021.

SOURAV DEV received the bachelor's degree in electrical and electronic engineering from Chittagong University of Engineering and Technology, Chittagong, Bangladesh, in 2013, and the master's degree in nanoelectronic systems from Technische Universität Dresden, Dresden, Germany, in October 2018, where he is currently pursuing the Ph.D. degree. In December 2018, he joined the Integrated Photonic Devices Group, Technische Universität Dresden, as a Research Associate. His current research interests include short-range optical communication based on photonic reservoir computing and the design of forward-biased Mach–Zehnder modulators for various applications.

KARANVEER SINGH received the integrated B.S. and M.S. degree in physical sciences and mathematical sciences as a minor from Indian Institute of Science Education and Research Thiruvananthapuram (IISER TVM), India, in 2018, and the Ph.D. degree in electrical engineering from Technische Universität Braunschweig, Germany, in 2024. His research interests include employing innovative optical signal processing on various silicon photonic platforms for optical communication and microwave photonics applications.

MIRCEA CATUNEANU received the B.E. degree in electrical and electronic engineering from the Politehnica University of Bucharest, Romania, in 2014, and the M.S. degree in nanoelectronic systems from Technische Universität Dresden, Germany, in 2017, where he is currently pursuing the Ph.D. degree with the Institut für Nachrichttechnik.

HRISHIKESH VITHALANI received the B.E. degree in electronics and communications engineering from the Babaria Institute of Technology, GTU, Vadodara, India, in 2018, and the M.S. degree in nanoelectronic systems from Technische Universität Dresden, Germany, in 2021, where he is currently pursuing the Ph.D. degree with the Institut für Nachrichttechnik. His research interests include modeling, simulating, and characterizing photonics integrated circuits (PIC) chips.

ABHINAND VENUGOPALAN received the B.S. and M.S. degrees in physical sciences and mathematical sciences as a minor from Indian Institute of Science Education and Research Thiruvananthapuram (IISER TVM), India, in 2022. He is currently pursuing the Ph.D. degree with the Institut für Hochfrequenztechnik, Technische Universität Braunschweig, Braunschweig, Germany.

JANOSCH MEIER received the B.Sc. and M.Sc. degrees in physics from Technische Universität Braunschweig, Germany, in 2015 and 2016, respectively. Since 2017, he has been a Research Assistant with the Terahertz-Photonics Group, Institut für Hochfrequenztechnik, Technische Universität Braunschweig. His current research interests include optical signal processing, especially photonic digital-to-analog and analog-to-digital conversion.

THOMAS SCHNEIDER received the Diploma degree in electrical engineering from Humboldt-Universität zu Berlin, Berlin, Germany, in 1995, and the Ph.D. degree in physics from Brandenburgische Technische Universität Cottbus–Senftenberg, Cottbus, Germany, in 2000. From 2000 to 2013, he was with Deutsche Telekom Hochschule für Telekommunikation (HfT), Leipzig, Germany. From 2006 to 2013, he was the Head of the Institut für Hochfrequenztechnik, HfT. Since 2014, he has been the Head of the Terahertz-Photonics-Group, Institut für Hochfrequenztechnik, Technische Universität Braunschweig, Braunschweig, Germany. His current research interests include nonlinear optical effects in telecommunication systems and sensors, slow and fast light, high-resolution spectroscopy, the generation of millimeter and THz waves, optical sampling, and integrated photonics.

KAMBIZ JAMSHIDI (Senior Member, IEEE) received the Ph.D. degree in electrical engineering from the Sharif University of Technology (SUT), Tehran, Iran, in 2006. From 2006 to 2009, he was with the Advanced Communication Research Institute (ACRI), SUT, as a Researcher. From 2009 to 2012, he was a Senior Researcher with the High-Frequency Technology (HFT) Institute, Deutsche Telekom University of Applied Sciences, Leipzig, Germany. From 2012 to 2013, he was with the HFT Institute and the Photonics Laboratory, Technical University of Berlin (TU Berlin). Since 2013, he has been an Assistant Professor with the Integrated Photonic Devices, Communications Laboratory, Faculty of Electrical and Computer Engineering, Technische Universität Dresden. He is a Senior Member of the Optical Society of America.